Sensors and Materials, Vol. 35, No. 6 (2023) 2101–2110
MYU Tokyo

S & M 3309

Variable-parameter Speed Controller for Adaptive Flux-vector-controlled Permanent Magnet Synchronous Motor Drive Using Improved Particle Swarm Optimization Algorithm

Yung-Chang Luo,* Song-Yi Xie, Chia-Hung Lin, and Ying-Piao Kuo

Department of Electrical Engineering, National Chin-Yi University of Technology,
No. 57, Sec. 2, Zhongshan Rd, Taiping Dist, Taichung 41170, Taiwan (ROC)

(Received December 28, 2022; accepted May 25, 2023)

Keywords: flux-vector-controlled (FVC), permanent magnet synchronous motor (PMSM) drive, improved particle swarm optimization (PSO) algorithm, adaptive speed prediction scheme, firefly algorithm (FA)

A variable-parameter speed controller was developed for an adaptive flux-vector-controlled (FVC) permanent magnet synchronous motor (PMSM) drive. The decoupled FVC PMSM drive was established using the stator voltage and current, and an adaptation mechanism of the model reference adaptive system (MRAS) speed prediction scheme was designed using the firefly algorithm (FA). A variable-parameter speed controller was designed using an improved particle swarm optimization (PSO) algorithm, replacing the conventional fixed-parameter speed controller to adapt to severe interference and sudden load changes. Hall-effect current sensors were used as electromagnetic sensing elements to detect the stator current from the PMSM. A MATLAB/Simulink© toolbox was used to establish the simulation scheme, and all control algorithms were realized using a microcontroller card. Simulation and experimental results under load changes confirmed the effectiveness of the proposed approach.

1. Introduction

The development of electric vehicles and high-precision machinery industries requires many high-performance motors as actuators. Compared with other types of motors, permanent magnet synchronous motors (PMSMs) have advantages of energy saving, small volume, and robustness, and are widely selected as drive motors by the above-mentioned industries. According to the PMSM flux vector control theory, the complicated PMSM mathematical model can be distributed into flux-current and torque-current components by coordinate transformation between a three-phase reference frame and a two-axis synchronous reference frame. Both components are orthogonal and the torque-current component is controllable, resulting in the attained maximum torque-to-current ratio. The realization of a conventional flux-vector-controlled (FVC) PMSM drive requires an encoder to detect the position of the rotor shaft. However, this sensor reduces drive robustness and is unsuitable in a hostile environment. The

*Corresponding author: e-mail: luoyc@ncut.edu.tw
https://doi.org/10.18494/SAM4290

ISSN 0914-4935

development of a speed prediction approach is necessary to replace the conventional FVC PMSM drive. The speed controller of the conventional FVC PMSM drive is designed with fixed parameters, and the performance will deteriorate owing to severe external interference and considerable load changes. Several speed-controller design methods with variable parameters of FVC PMSM drives, such as the variable-parameter identification via adaptive control system scheme,[1–4] variable-parameter adjustment dependent on a neural network,[5–7] variable-parameter design by an optimal control theory,[8,9] variable-parameter determination using a robust control method,[10–12] and variable-parameter estimation from a fuzzy logic control, have been published.[13–15] These methods are rarely used in the speed prediction FVC PMSM drive. In this research, the speed controller of an adaptive speed prediction FVC PMSM drive was designed with variable parameters to adapt to severe interference and sudden load changes. In the proposed FVC PMSM drive, a model reference adaptive system (MRAS) was used to develop a speed prediction scheme, and the adaptation mechanism of MRAS was designed using the firefly algorithm (FA). A time-varying speed controller was designed using an improved particle swarm optimization (PSO) algorithm to adapt to severe interference and sudden load changes, which has advantages of less computational burden, no training database, and easy design. The three-phase stator current measurement for the realization of the speed prediction scheme was acquired from a PMSM using Hall-effect current sensors.

This paper comprises six sections. In Sect. 1, we present the research motivation, background, and literature review on the variable-parameter speed controller of adaptive speed prediction FVC PMSM drives. In Sect. 2, we describe the proposed decoupled FVC PMSM drive. In Sect. 3, we discuss the development of the MRAS speed prediction scheme with the FA adaptation mechanism. The details of the design procedure of an improved PSO variable-parameter controller are given in Sect. 4. Sections 5 and 6 cover the experimental setup, results, discussion, and conclusion.

2. Decoupled FVC PMSM Drive

Suppose that the permanent magnets of a PMSM are surface-mounted on the rotor without damper winding and that the magnetic axis of the permanent magnets is consistent with the *d*-axis component of the rotor shaft. The two-axis stator dynamic equations of a PMSM in the synchronous reference coordinate frame are given by[16]

$$pi_{qs}^{e} = -(\omega_e R_s / X_s) i_{qs}^{e} - \omega_e i_{ds}^{e} - (\omega_e^2 / X_s)\lambda_{Fr} + (\omega_e / X_s) v_{qs}^{e}, \tag{1}$$

$$pi_{ds}^{e} = -(\omega_e R_s / X_s) i_{ds}^{e} + \omega_e i_{qs}^{e} + (\omega_e / X_s) v_{ds}^{e}, \tag{2}$$

where $p = d/dt$ is a differential operator; i_{qs}^{e} and i_{ds}^{e} are the *q*-axis and *d*-axis stator currents, v_{qs}^{e} and v_{ds}^{e} are the *q*-axis and *d*-axis stator voltages, and X_s and R_s are the reactance and resistance of the stator, respectively; λ_{Fr} is the equivalent rotor magnet flux linkage developed by the permanent magnets of the rotor; and ω_e is the speed of the synchronous reference coordinate frame.

An examination of Eq. (1) reveals that the second and third terms on the right side are the coupling components in relation to the *d*-axis stator current and equivalent rotor magnet flux linkage, respectively. Also, an examination of Eq. (2) reveals that the second term on the right side is a coupling component in relation to the *q*-axis stator current. On the basis of these coupling components, the *q*-axis and *d*-axis stator voltage feedforward compensations can be defined as

$$v_{qs\_cp}^{e} = \omega_e \lambda_{Fr} + X_s i_{ds}^{e}, \tag{3}$$

$$v_{ds\_cp}^{e} = -X_s i_{qs}^{e}. \tag{4}$$

Thus, the linear control of the *q*-axis and *d*-axis stator current loops can be acquired. The voltage commands of the *q*-axis and *d*-axis stator current control loops are given by

$$v_{qs}^{e*} = (\omega_e / X_s) v'_{qs} + (\omega_e / X_s) v_{qs\_cp}^{e}, \tag{5}$$

$$v_{ds}^{e*} = (\omega_e / X_s) v'_{ds} + (\omega_e / X_s) v_{ds\_cp}^{e}, \tag{6}$$

where v'_{qs} and v'_{ds} are the outputs of the *q*-axis and *d*-axis stator current controllers, respectively.

The developed electromagnetic torque of a PMSM is derived as

$$T_e = \left(P / 2\right) \lambda_{Fr} i_{qs}^{e}, \tag{7}$$

where P is the number of motor poles. Equation (7) reveals that the equivalent rotor magnet flux linkage λ_{Fr} and *q*-axis stator current i_{qs}^{e} are orthogonal. The generated electromagnetic torque of a PMSM is controlled by i_{qs}^{e}, and the maximum torque-to-current ratio is attained. The mechanical equation of a PMSM is acquired as

$$T_e = J_m p \omega_{rm} + B_m \omega_{rm} + T_L, \tag{8}$$

where B_m and J_m are the viscous friction coefficient and inertia of the PMSM, respectively, T_L is the load torque, $\omega_{rm} = (2/P)\omega_r$ is the mechanical speed of the motor shaft, and ω_r is the rotor electric speed of the PMSM.

3. MRAS Speed Prediction Scheme

In this study, the speed prediction scheme was established in accordance with an MRAS based on the reactive power of a PMSM, and the adaptation mechanism of the MRAS was developed using the FA.

According to the MRAS theory,[17] the reference model and the adjustable model based on the reactive power of a PMSM can be derived as Eqs. (9) and (10), respectively.

$$Q = v_{qs}^{e} i_{ds}^{e} - v_{ds}^{e} i_{qs}^{e}, \tag{9}$$

$$Q' = \hat{\omega}_e \left[(X_s / \omega_e)(i_{ds}^{e})^2 + \lambda_{Fr} i_{ds}^{e} + (X_s / \omega_e)(i_{qs}^{e})^2 \right], \tag{10}$$

where " ˆ " implies an identified value. The difference between the reference and adjustable models is applied to an adaptation mechanism to identify $\hat{\omega}_e$. Figure 1 shows the established MRAS rotor speed prediction scheme. Here, the synchronous position angle for the coordinate transformation between the two-axis synchronous coordinate frame and the three-phase system ($2^e \Rightarrow 3$ and $2^e \Leftarrow 3$) is given by

$$\hat{\theta}_e = \frac{1}{s} \hat{\omega}_e, \tag{11}$$

where s is a Laplace operator.

The adaptation mechanism of the MRAS was developed using FA, which has the advantages of easy understanding, relatively few setting parameters, and easy implementation. Figure 2 shows the flow chart of the proposed FA-design procedure, which includes the setting of parameters, the initialization of the firefly position and brightness, updating the firefly position and brightness, and the evaluation of the obtained new solution.[18]

4. Variable-parameter Speed Controller Using an Improved PSO Algorithm

In dynamic situations, the conventional PSO algorithm with a fixed inertia weight will cause particles to fall into the best solution at the previous time. A dynamic inertia-weighted PSO algorithm with perception and response can update the best solution of particles at the present

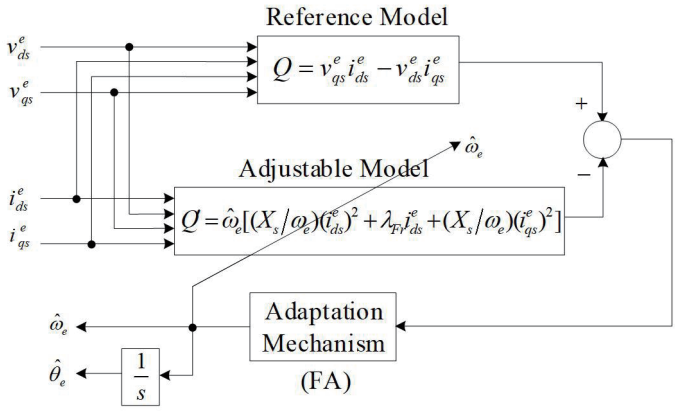

Fig. 1. MRAS rotor speed prediction scheme based on the reactive power.

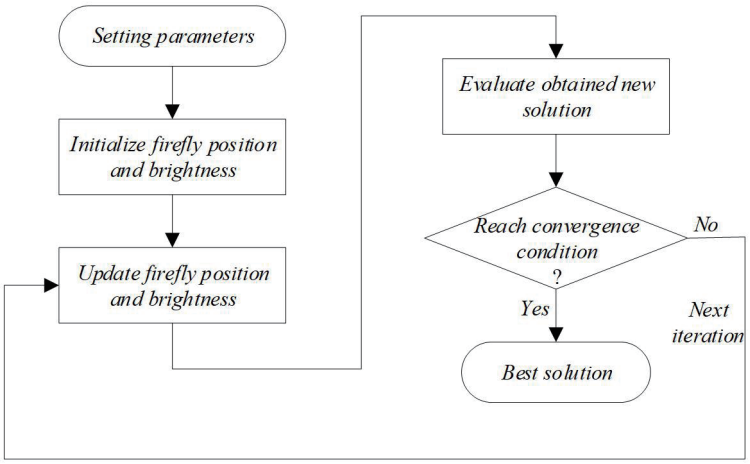

Fig. 2. Flow chart of the proposed adaptation mechanism design using FA.

time. The dynamic inertia-weighted PSO algorithm senses current external changes to update the particles in response to the changes.[19,20] Particles with a large inertia weight have a strong large-scale search as a global search, while particles with a small inertia weight have a strong small-scale search as a local search. In the initial stage of the algorithm, the global search can quickly obtain the global best solution area, and the local search can quickly obtain the best solution of the problem by linearly reducing the inertia weighting in the final stage of the algorithm. In this research, an improved PSO algorithm with a dynamic inertia weight was used to predict proportional and integral gains (K_{ps}, K_{is}) for the variable-parameter speed controller. In the dynamic inertia-weighted PSO algorithm, a reiterative computation procedure is applied to update the velocity and position of each particle until the termination condition is satisfied for the best solution. The updated velocity and position of the particle are given by

$$v_i(n+1) = w \cdot v_i(n) + \alpha_1 \cdot rand \cdot (P_{best}(n) - x_i(n)) + \alpha_2 \cdot rand \cdot (G_{best}(n) - x_i(n)), \tag{12}$$

$$\alpha_1 = (\alpha_{1max} - \alpha_{1min}) \cdot m / m_{max}, \tag{13}$$

$$\alpha_2 = (\alpha_{2max} - \alpha_{2min}) \cdot m / m_{max}, \tag{14}$$

$$w = w_{max} - (w_{max} - w_{min}) \cdot m / m_{max}, \tag{15}$$

where $v_i(n)$ and $v_i(n + 1)$ are the present and next particle velocities, respectively. Moreover, $x_i(n)$ is the present position of the particle, w is a weighting factor, and *rand* is a random: P_{best} and G_{best} are the best positions of the individual particle and swarm, α_1 and α_2 are the learning factors of the individual particle and swarm, α_{1max} and α_{2max} are the initial learning factors of the individual particle and swarm, α_{1min} and α_{2min} are the terminal learning factors of the

individual particle and swarm, w_{max} and w_{min} are the initial and terminal weighting factors, and m and m_{min} are the present and maximum iteration numbers, respectively. Figure 3 shows the flow chart of the proposed variable-parameter speed controller using the dynamic inertia weighting PSO algorithm.

Figure 4 shows the block diagram of the proposed variable-parameter speed controller for the adaptive FVC PMSM drive. The drive includes a variable-parameter speed controller, q-axis and d-axis stator current controllers, q-axis and d-axis stator voltage decoupling, coordinate transformation between synchronous and stationary reference frames ($2^e \Rightarrow 3$, $2^e \Leftarrow 3$), MRAS speed prediction using the FA adaptation mechanism, and an improved PSO algorithm speed controller design scheme. In this research, the proportional-integral (P-I) controllers for q-axis and d-axis stator current control loops were designed according to the root-locus and Bode plot. The improved PSO algorithm speed controller was designed by dynamic inertia weighting. Then, the three-phase currents (i_{as}, i_{bs}, and i_{cs}) were obtained from the PMSM using Hall-effect current sensors that achieved the coordinate transformation from a three-phase reference frame to a two-axis synchronous reference frame ($2^e \Leftarrow 3$).

5. Experimental Setup and Results

A simulation scheme of the proposed system was established using the MATLAB/Simulink© toolbox. The implementation program was executed using a TI DSP 6713-and-F2812 control card and a voltage source inverter to actuate the PMSM. A standard three-phase, 220 V, 0.75 kW, Y-connected PMSM was used to confirm the effectiveness of the proposed variable-parameter speed controller for the adaptive FVC PMSM drive using the improved PSO algorithm. In a running cycle, the sequence of speed commands was designed as follows: forward-direction

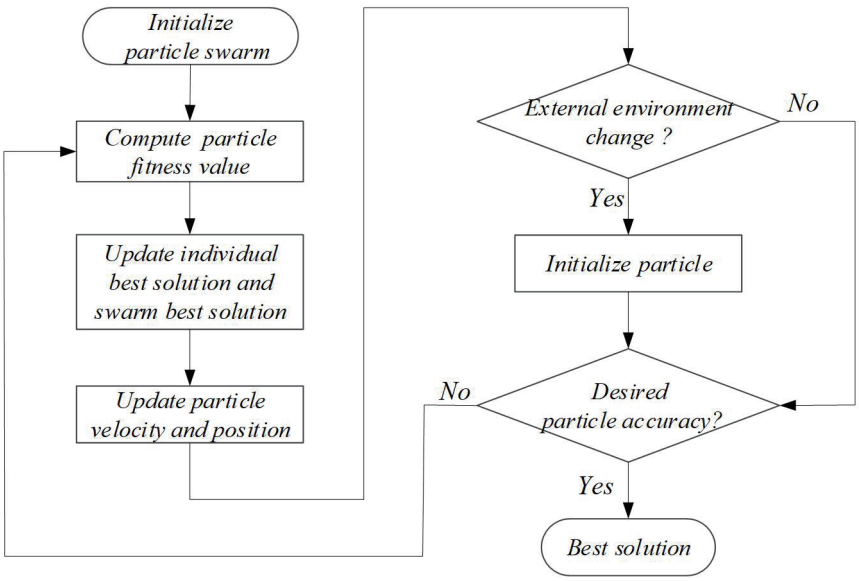

Fig. 3. Flow chart of the proposed variable-parameter speed controller using the improved PSO algorithm.

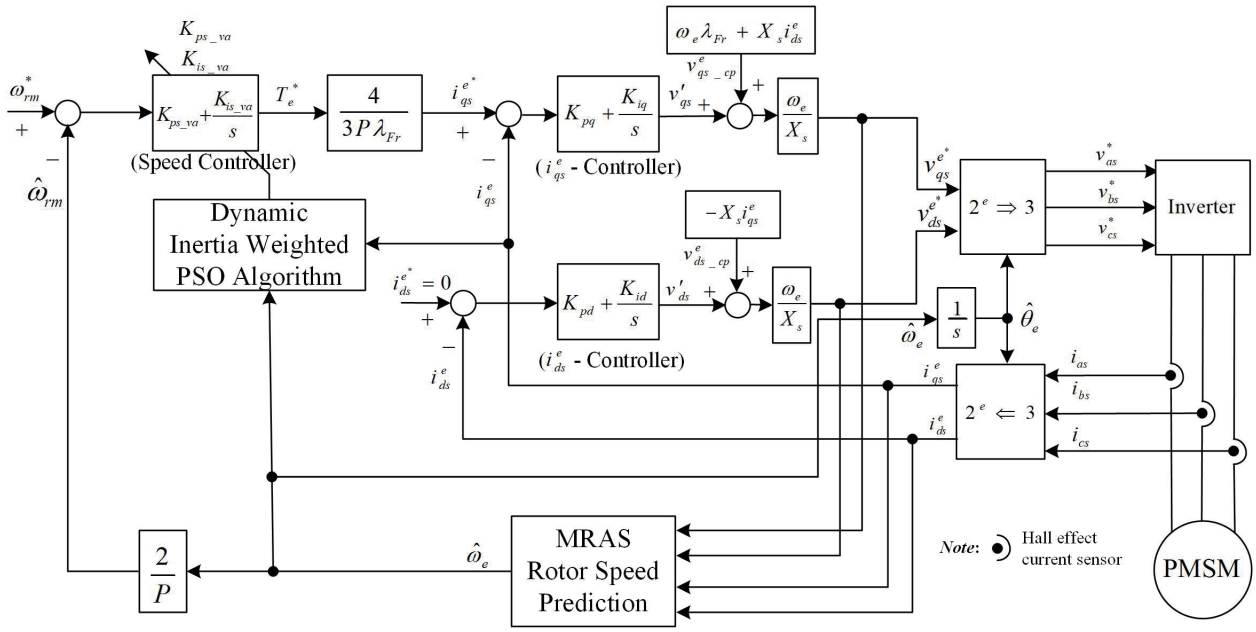

Fig. 4. Variable-parameter speed controller for the adaptive FVC PMSM drive using the improved PSO algorithm.

acceleration from $t = 0$ s to $t = 1$ s, forward-direction steady-state running at the interval $1 \le t \le 7$ s, forward-direction braking to reach the zero speed during $7 \le t \le 8$ s, reverse-direction acceleration from $t = 8$ s to $t = 9$ s, reverse-direction steady-state running at the interval $9 \le t \le 15$ s, and reverse-direction braking to reach zero speed during $15 \le t \le 16$ s. Furthermore, in the running cycle, load changes were designed as follows: in the forward-direction steady-state running at the interval $1 \le t \le 7$ s, no load was added over $1 \le t \le 3$ s, a 3 N-m load was added from $t = 3$ s to $t = 4$ s, no load was added over $4 \le t \le 5.5$ s, a 2.5 N-m load was added from $t = 5.5$ s to $t = 6.5$ s, and no load was added over $6.5 \le t \le 7$ s; in the reverse-direction steady-state running at the interval $9 \le t \le 15$ s, no load was added over $9 \le t \le 11$ s, a 3 N-m load was added from $t = 11$ s to $t = 12$ s, no load was added over $12 \le t \le 13.5$ s, a 2.5 N-m load was added from $t = 13.5$ s to $t = 14.5$ s, and no load was added over $14.5 \le t \le 15$ s.

Figures 5 and 6 illustrate the simulation and experimental results with steady-state load changes for a reversible steady-state speed command of 1800 rev/min, respectively. Each figure includes eight responses: (a) variable proportional gain parameter, (b) variable integral gain parameter, (c) command (dashed line) and predicted (solid line) rotor speed, (d) command (dashed line) and actual (solid line) rotor speed, (e) synchronous position angle, (f) stator flux locus (q-axis vs d-axis), (g) electromagnetic torque, and (h) stator current.

According to the simulation and experimental test results under reversible operations and steady-state load change conditions, the developed MRAS with an FA adaptation mechanism could accurately predict the rotor speed, and the designed variable-parameter speed controller using an improved PSO algorithm could properly adapt steady-state load changes. Furthermore, the promising responses of electromagnetic torque and stator current were achieved, and the

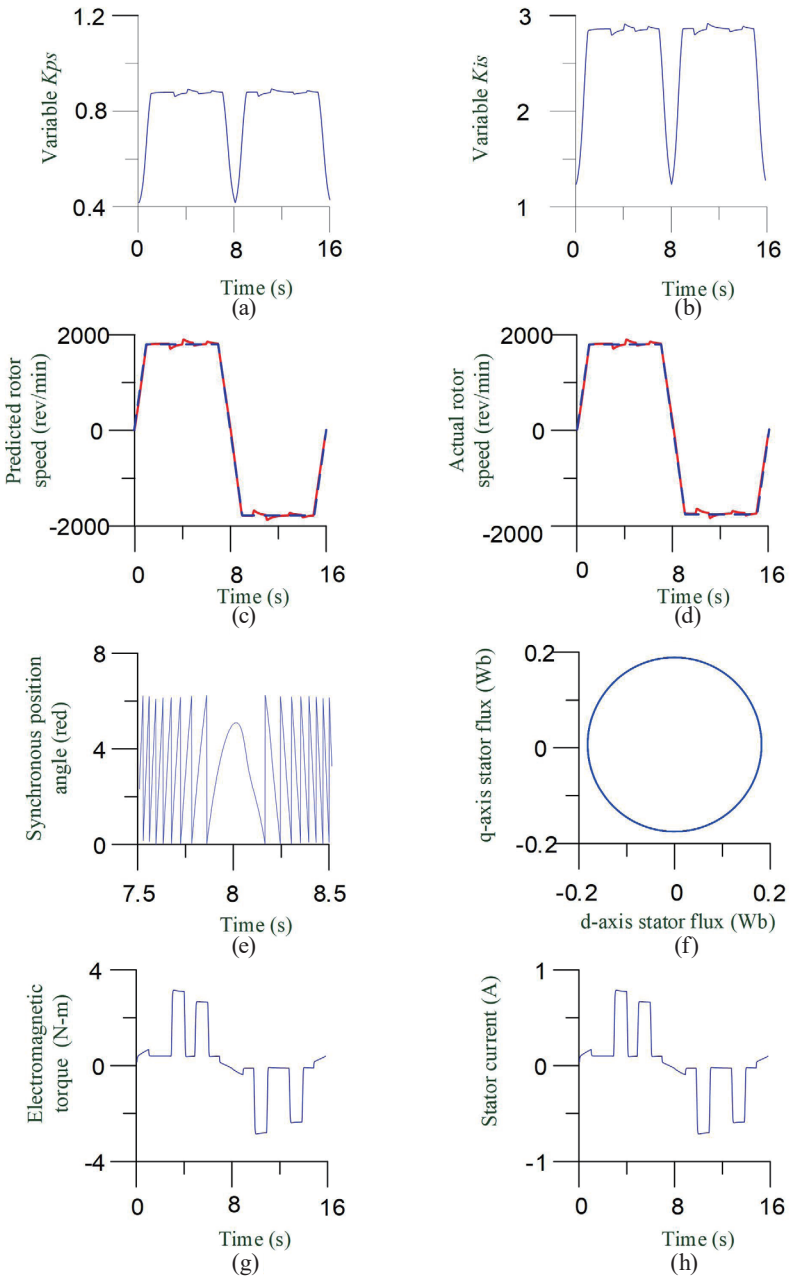

Fig. 5. (Color online) Simulated responses of the proposed variable-parameter speed controller for the adaptive FVC PMSM drive using an improved PSO algorithm with load changes for a reversible steady-state speed command of 1800 rev/min: (a) variable proportional gain parameter, (b) variable integral gain parameter, (c) predicated rotor speed, (d) actual rotor speed, (e) synchronous position angle, (f) stator flux locus, (g) electromagnetic torque, and (h) stator current.

sawtooth synchronous position angle and circular steady-state stator flux locus confirmed the correct coordinate transformation to be achieved.

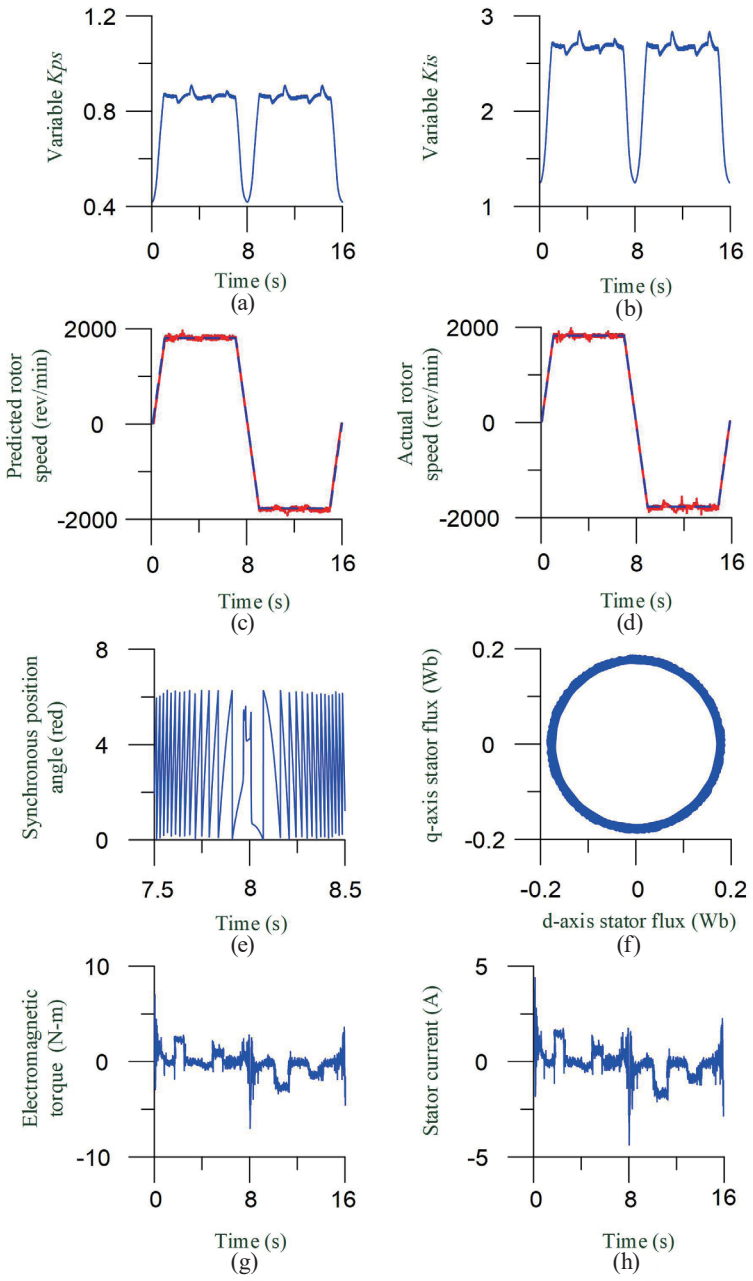

Fig. 6. (Color online) Experimental responses of the proposed variable-parameter speed controller for the adaptive FVC PMSM drive using an improved PSO algorithm with load changes for reversible steady-state speed command of 1800 rev/min: (a) variable proportional gain parameter, (b) variable integral gain parameter, (c) predicated rotor speed, (d) actual rotor speed, (e) synchronous position angle, (f) stator flux locus, (g) electromagnetic torque, and (h) stator current.

6. Conclusions

A variable-parameter speed controller using an improved PSO was developed for an adaptive FVC PMSM drive. The decoupled FVC PMSM drive was established according to the current

and voltage of the stator. The dynamic inertia-weighted PSO algorithm was used to design the speed controller with variable P-I gain parameters. The MRAS with an FA adaptation mechanism was used to predict the rotor speed. Three-phase stator currents for implementing the variable-parameter speed controller for adaptive FVC PMSM drives were provided by Hall-effect current sensors. Simulation and experimental results for reversible steady-state speed commands under steady-state load changes confirmed the promising performance of the proposed variable-parameter speed controller for the adaptive FVC PMSM drive.

References

1 S. Cheng, Y. Y. Huang, and H. H. Chou: Proc. 2008 ECSIS Learning Adaptive Behaviors Robotic Systems Symp. (ECSIS, 2008) 97–102. https://doi.org/10.1109/LAB-RS.2008.27
2 W. Xu, M. M. Ismail, Y. Liu, and M. R. Islam: IEEE Trans. Pow. Electro. **34** (2019) 1218. https://doi.org/10.1109/TPEL.2019.2908380
3 Y. A. R. I. Mohamed: IEEE Trans. Energy Conver. **22** (2007) 829. https://doi.org/10.1109/TEC.2007.895869
4 C. Wang and Z. Q. Zhu: IEEE Trans. Ind. Appl. **56** (2020) 1505. https://doi.org/10.1109/TIA.2020.2967673
5 Y. Wang, J. G. Zhu, and Y. G. Guo: Proc. 2007 Australasian Universities Power Engineering Conf. (AUPEC, 2007) 1–5. https://doi.org/10.1109/AUPEC.2007.4548041
6 Li, Z. Gu, and J. Tian: Proc. 2016 Chinese Control and Decision Conf. (CCDC, 2016) 3061–3064. https://doi.org/10.1109/CCDC.2016.7531507
7 Y. Yi, D. M. Vilathgamuwa, and M. A. Rahman: Proc. IEEE Industry Applications Conf. (IAS, 2001) 945–952. https://doi.org/10.1109/IAS.2001.955566
8 M. Liu, K. W. Chan, J. Hu, W. Xu, and J. Rodriguez: IEEE Trans. Ind. Inf. **15** (2019) 4944. https://doi.org/10.1109/TII.2019.2898004
9 L. Yan, M. Dou, Z. Hua, H. Zhang, and J. Yang: IEEE Trans. Pow. Electro. **34** (2019) 2784. https://doi.org/10.1109/TPEL.2018.2842743
10 D. Liu, C. Che, and Z. Zhou: Proc. 2011 Int. Mechatronic Science, Electric Engineering and Computer Conf. (MEC, 2011) 8–11. https://doi.org/10.1109/MEC.2011.6025388
11 M. Kashif, S. Murshid, and B. Singh: Proc. 2018 2nd Int. Power Electronics, Intelligent Control and Energy Systems Conf. (ICPEICES, 2018) 765–770. https://doi.org/10.1109/ICPEICES.2018.8897369
12 Y. A. R. I. Mohamed: IEEE Trans. Ind. Electro. **54** (2007) 2864. https://doi.org/10.1109/TIE.2007.901356
13 A. J. Abianeh: Proc. 2011 6th IEEE Industrial Electronics and Applications Conf. (ICIEA, 2011) 657–662. https://doi.org/10.1109/ICIEA.2011.5975668
14 X. Cao and L. Fan: Proc. 2009 Int. Mechatronics and Automation Conf. (ICMA, 2009) 1228–1232. https://doi.org/10.1109/ICMA.2009.5246561
15 X. Cao and L. Fan: Proc. 2009 IITA Int. Control, Automation and Systems Engineering Conf. (CASE, 2009) 287–290. https://doi.org/10.1109/CASE.2009.89
16 C. H. Liu: Control of AC Electrical Machines (Tunghua, Taipei, 2008) 4th ed., Chap. 6 (in Chinese).
17 A. Pal, S. Das, and A. K. Chattopadhyay: IEEE Trans. Pow. Electro. **33** (2018) 5131. https://doi.org/10.1109/TPEL.2017.2657648
18 M. K. Merugumalla and P. K. Navuri: Proc. 2018 2nd Int. Inventive Systems and Control Conf. (ICISC, 2018) 994–999. https://doi.org/10.1109/ICISC.2018.8398951
19 J. C. Bansal, H. Sharma, S. S. Jadon, and M. Clerc: Memetic Comput. **6** (2014) 31. https://doi.org/10.1007/s12293-013-0128-0
20 D. Wang, J. Fan, Z. Xiao, H. Jiang, H. Chen, F. Zeng, and K. Li: IEEE Trans. Intel. Transp. Sys. **20** (2019) 3623. https://doi.org/10.1109/TITS.2018.2878253